Envisat Altimetry Radar Waveform Retracking of Quasi-Specular Echoes over the Ice-Covered Qinghai Lake

Kuo-Hsin Tseng[1,*], C. K. Shum[1], Yuchan Yi[1], Hok Sum Fok[1], Chung-Yen Kuo[2], Hyongki Lee[3], Xiao Cheng[4], and Xianwei Wang[5]

[1] *Division of Geodetic Science, School of Earth Sciences, Ohio State University, Columbus, Ohio, USA*
[2] *Department of Geomatics, National Cheng-Kung University, Tainan, Taiwan*
[3] *Department of Civil and Environmental Engineering, University of Houston, Houston, Texas, USA*
[4] *College of Global Change and Earth System Science, Beijing Normal University, Beijing, China*
[5] *State Key Laboratory of Remote Sensing Science, Institute of Remote Sensing Applications,*
Chinese Academy of Sciences, and Beijing Normal University, Beijing, China

ABSTRACT

The use of satellite radar altimetry has long been extended to areas other than the deep-ocean primarily because of the advances in radar waveform retracking methodologies. However, the retracking algorithms are limited to a handful shapes of return echoes over assumed known surfaces, while numerous unknown waveforms exist due to the complexity of real-world land cover and other surfaces. Measurements over a surface with seasonal or ephemeral patterns could thus degrade in accuracy due to varying characteristics from the corresponding radar backscatters. In this study, we demonstrate that the Qinghai Lake, an alpine water body with distinct seasonal variation between water and ice causes inaccurate surface-height estimates when using Envisat radar altimetry and conventional retracking techniques. Following the characterization of the lake surface using EO-1 and Landsat multispectral analysis, we hypothesize that the overestimation of the lake level during winter and early spring is not from the snow accumulation; rather it is due to an error of the onboard retracker (ICE-1) which is unable to properly model the quasi-specular waveforms. Hence, we first build a classification algorithm to identify the anomalous waveforms, and then use an empirical retracking gate correction to mitigate the ice contamination. The accuracy of the 20% threshold retracker (TR) after applying suggested gate correction has a significant improvement with a root-mean-square error (RMSE) of 6 ± 7 cm and a correlation of 0.98 compared with the *in situ* gauge data. The improvement in accuracy is 54% better than the ICE-1 and 85% than the OCEAN retrackers, respectively.

Key words: Qinghai Lake water level, Tibetan Plateau, Satellite altimetry, Waveform retracking, Specular echoes, Lake ice
Citation: Tseng, K. H., C. K. Shum, Y. Yi, H. S. Fok, C. Y. Kuo, H. Lee, X. Cheng, and X. Wang, 2013: Envisat altimetry radar waveform retracking of quasi-specular echoes over the ice-covered Qinghai Lake. Terr. Atmos. Ocean. Sci., 24, 615-627, doi: 10.3319/TAO.2012.12.03.01(TibXS)

1. INTRODUCTION

Satellite altimetry has long been a promising tool for studies over the deep ocean (Shum et al. 1995; Fu and Cazenave 2001), coastal ocean (Vignudelli et al. 2009; Lee et al. 2010), inland hydrology (Birkett 1995; Koster et al. 1999; Shum et al. 2003; Berry et al. 2005; Calmant and Seyler 2006; Zhang et al. 2010; Hwang et al. 2011; Kuo and Kao 2011), vertical crustal motion (Lee et al. 2008), ice sheet and sea ice freeboard elevation changes (Zwally et al. 1989; Bamber 1994; Wingham et al. 1998; Kwok et al. 2009; Lee et al. 2012). These extended applications have been possible due in part to the advances in radar waveform retracking methodologies (Frappart et al. 2006). Although the dual-frequency radar altimeter waveform is not compatible with Brown's theoretical model (Brown 1977) over non-marine surfaces, various retrackers (Martin et al. 1983; Wingham 1986; Bamber 1994; Davis 1997; Lee et al. 2008) have been developed to adjust telemetered range from various heterogeneous surfaces by modeling the anomalous waveforms with specific functions and estimating track offset (the difference between nominal tracking gate and the actual retracked gate) at a preset power amplitude along the leading edge.

---

* *Corresponding author*
  E-mail: tseng.95@osu.edu

Notably, it is widely accepted that there is no single unsupervised retracker is able to effectively retrieve accurate heights over all surface types, no matter whether it is model-based or empirical algorithm. Instead, physical or empirical retrackers are usually suitable for only certain types of land, ice or water topography. Seasonal or ephemeral variation in surface conditions, e.g., water in summer and icy surface in winter for a lake, is somewhat overlooked by specific retrackers that could potentially be subject to errors in estimate of surface level variation (Jiang et al. 2008). Furthermore, existing retrackers were mostly developed on the basis of Brown's hypothesized condition for a deep ocean surface echo with a predetermined shape of leading or trailing edge, and an ideal radar waveform return from an aver-age of a flat surface. In contrast to Brown's assumption of scattering processes for an isotropic footprint over a rough ocean surface with waves, it is certain that this template is not applicable for calm or frozen lakes, or for other high reflectivity surfaces with extreme specular nature (Dinardo and Benveniste 2009; Idris and Deng 2011). Therefore, the purpose of this research is to develop an algorithm, which allows to automatically detect specular shapes of waveform returns and empirically correct the retracked gate for the distorted waveforms.

This study is conducted using European Space Agency (ESA)'s Envisat satellite altimetry with 35-day repeat orbits over the Qinghai Lake which is located northeast of the Qinghai-Tibetan Plateau, China (Fig. 1a). The Qinghai
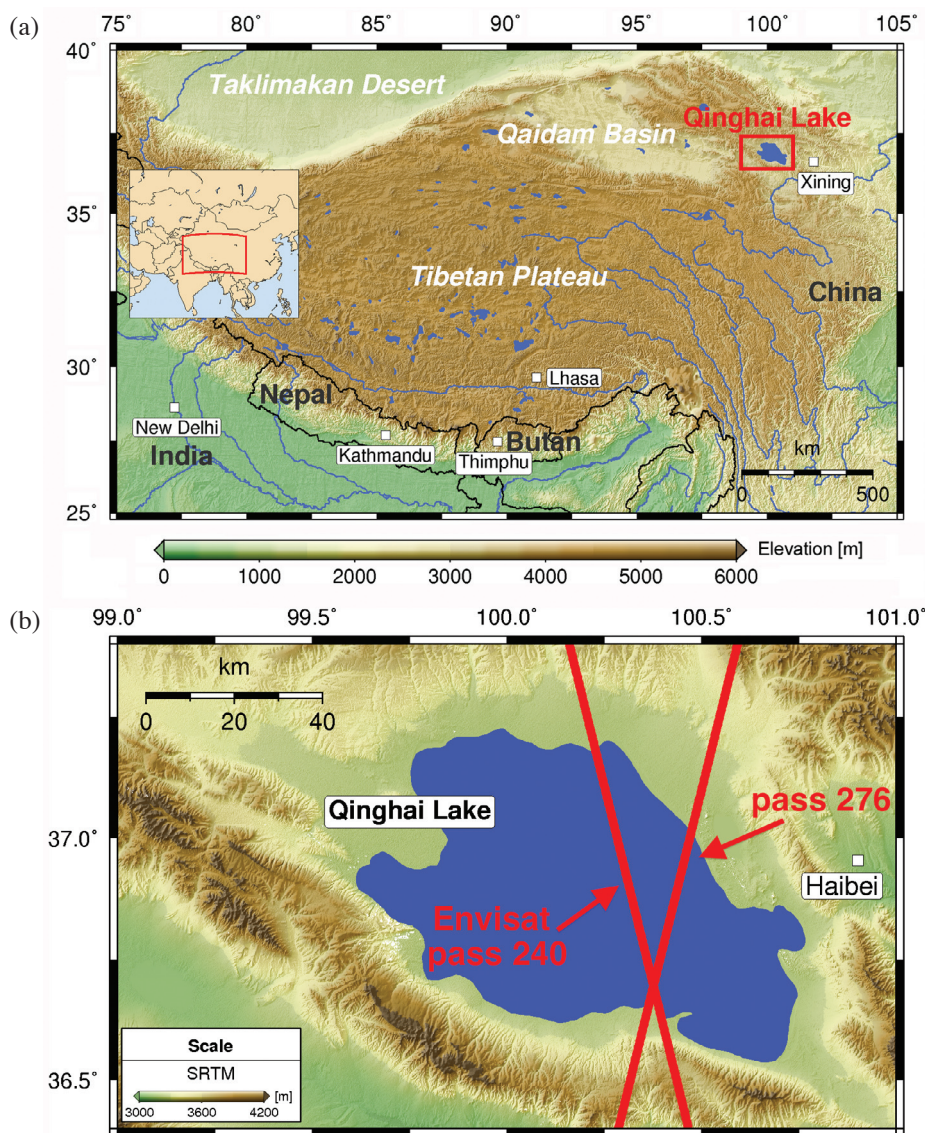

Fig. 1. (a) Location of the Qinghai Lake on the Tibetan Plateau (red box). The topographic relief is scaled by GTOPO30 DEM. (b) Two Envisat passes #240 and #276 (red) are included in this study. SRTM 3 arc-second C-band DEM is used as a topographic relief. The lake boundary refers to the World Vector Shorelines (WVS) and CIA World Data Bank II (WDBII) composed by the Generic Mapping Tools (GMT) (Wessel and Smith 2010).

Lake at an altitude of ~3000 m is the largest (saline) lake in China with seasonal changes in surface conditions (Che et al. 2009). We adopted two of three Envisat passes (#240 ascending and #276 descending) both of which have longer passes over the lake (Fig. 1b). Figure 2 shows that the time evolution of Envisat pass #240 backscattering coefficients (BC, representing the surface reflectivity and corresponding to the return waveform power) over the Qinghai Lake archived in the Envisat Geophysical Data Record (GDR). The BCs have intermittent blooms (> 20 dB) every year during the winter to early spring over the Qinghai Lake, matching pretty well with the ice freeze-up and break-up in time as observed by Moderate Resolution Imaging Spectroradiometer (MODIS) reflectance data (Che et al. 2009). We also note that the along-track altimeter waveforms variation have classifiable patterns which can be roughly separated in terms of surface conditions and corresponding months (Fig. 3). In Lee et al. (2011), the Envisat-measured lake level anomaly using the ICE-1 or the OCOG retracker (Wingham et al. 1986) over the Qinghai Lake has an apparent winter-peak pattern every year (Fig. 4) which is substantially different from available lake gauge data (Zhang et al. 2011a, b), with a consistently large amplitude difference of ~25 cm. There also have been reported studies that the lake ice in winter leads to higher surface height measurements for pulse-limited radar altimetry, e.g., Chu et al. (2007) using TOPEX/POSEIDON and Jiang et al. (2008) using Envisat altimetry data. However, this unmatched phenomenon is not evident in Zhang et al. (2011b) using ICESat laser altimetry, presumably also because that ICESat data could not continuously observe the seasonal variation of the lake

level due to instrument problem or data outages. Here, we hypothesize that the winter peak in the Envisat ICE-1 retracked lake level time series with regular annual pattern is caused by spurious radar returns resulting in erroneously retracked heights, instead of geophysical causes. The purpose of this study is to investigate the possible error in the waveform retracking for Envisat radar altimeter data that has led to the inconsistency. A comparison between a normal Brown-like waveform over Qinghai Lake water and a specular return from the frozen surface is shown in Fig. 5. The Brown-like return exemplified in Fig. 5 is an along-track average (within the latitudinal boundary of the study region) of Envisat pass #240, cycle 42, on 11/10/2005. The quasi-specular ice return is a single 18-Hz waveform taken from pass #240, cycle 33 measurement near latitude 36.917°N on 30 December 2004. A concentration of energy near the nominal tracking gate at 46 generates a sharp leading edge with a rapid decay, tilts the center of gravity (COG) of the whole waveform frontward and amplifies the kurtosis for the specular part. If the incompatibilities were ignored in the waveform retracking process, the estimate would shorten the telemetered range and therefore the ellipsoidal height on the target surface could be overestimated, under the assumption that the lake level of snow-free frozen surface is equivalent to the true water level. Similar phenomenon has been discussed in Dinardo and Benveniste (2009) and Idris and Deng (2011) for Envisat and Jason-1/-2 altimetry retracking along coastal regions. Their studies examined waveforms at a coastal region with quasi-specular shapes and developed a model-based algorithm to fit single or multi-peaks patterns. Therefore, it is suspected that a correction or modification
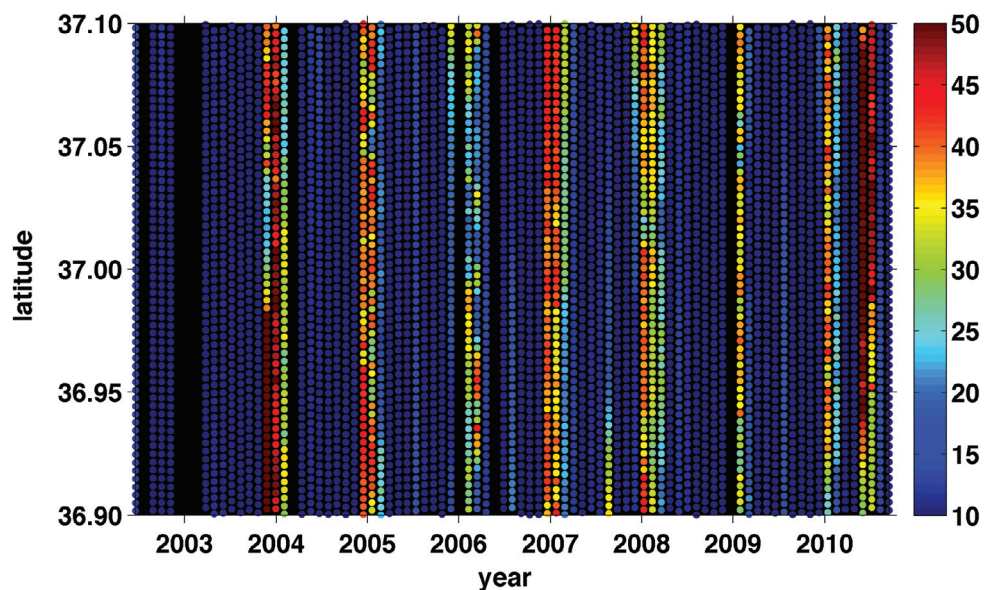

Fig. 2. Along-track (ordinate) variation of the Envisat pass #240 backscattering coefficient (BC, unit: [dB]) in time (abscissa). BC blooms are often noted in December, January, and February each year when the lake becomes icy with the least surface roughness and higher reflectivity. Some cycles are missing (e.g., early in 2003) due to data outage, a lost-lock in altimeter, or data failed to meet the edit criteria.
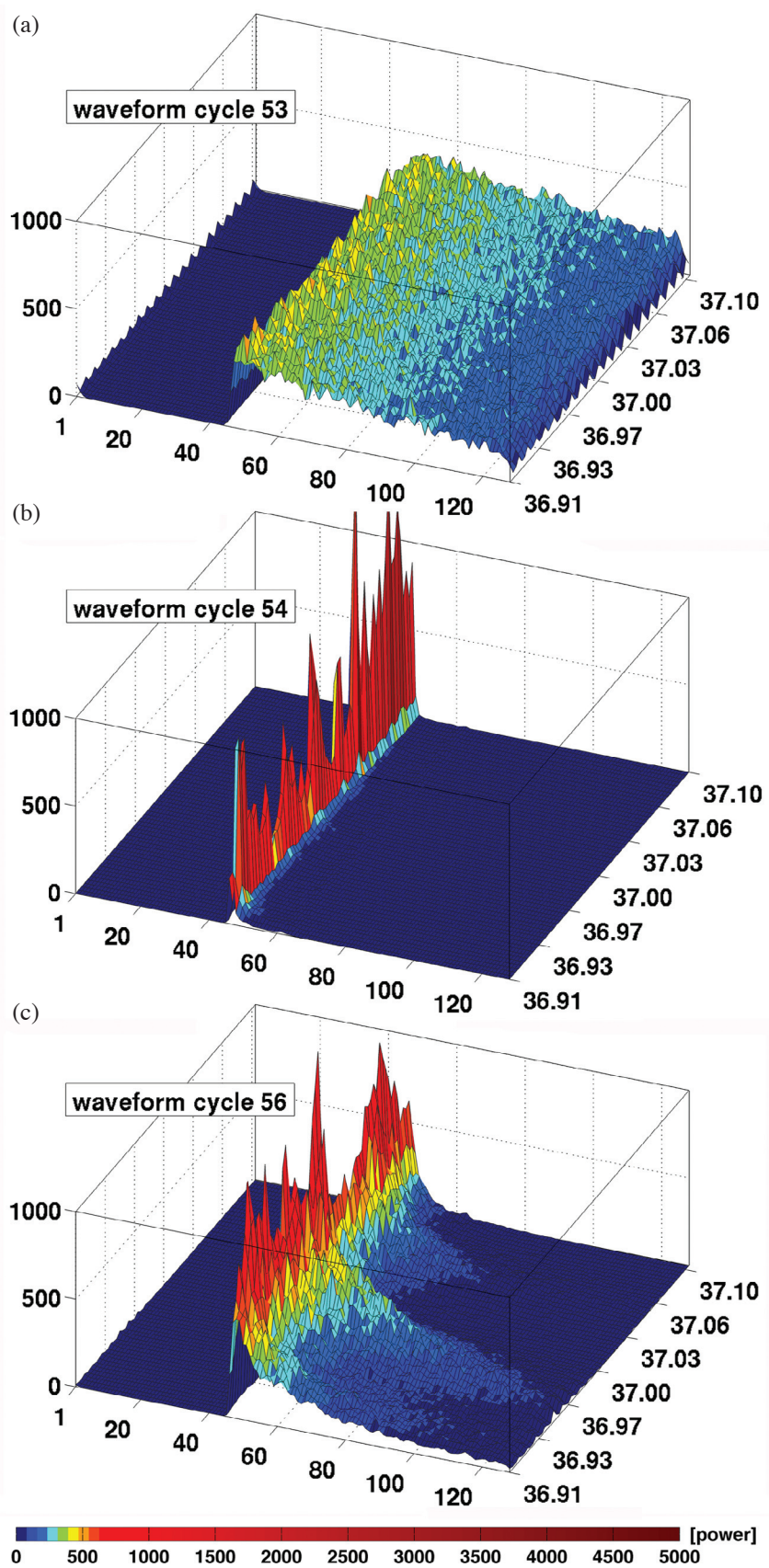
Fig. 3. Typical along-track waveforms returned from different surface conditions and corresponding months: (a) water (April - November), (b) ice (December - March), and (c) water with ice floes (March and December). X-axis is waveform gates (or bins), Y-axis indicates latitude in degree, and Z-axis indicates returned energy in power unit. These samples are demonstrated by Envisat pass #240 in cycles [from (a), (b), (c)] 53, 54, and 56.
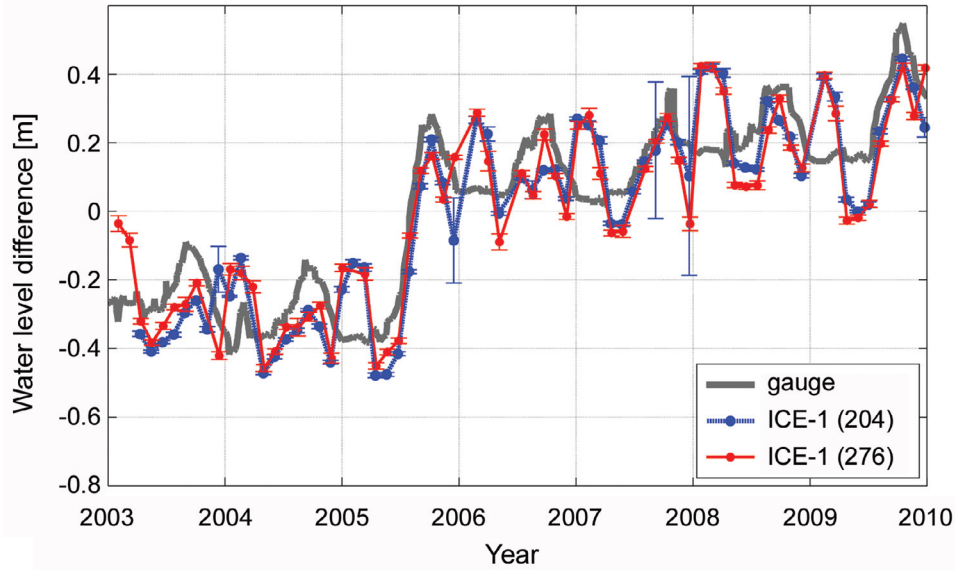
Fig. 4. Envisat ICE-1 retracked water level variation similar to Lee et al. (2011). Pass #240 (blue) and pass #276 (red) are computed from an along-track average within each latitudinal box and a regular 2σ editing process.
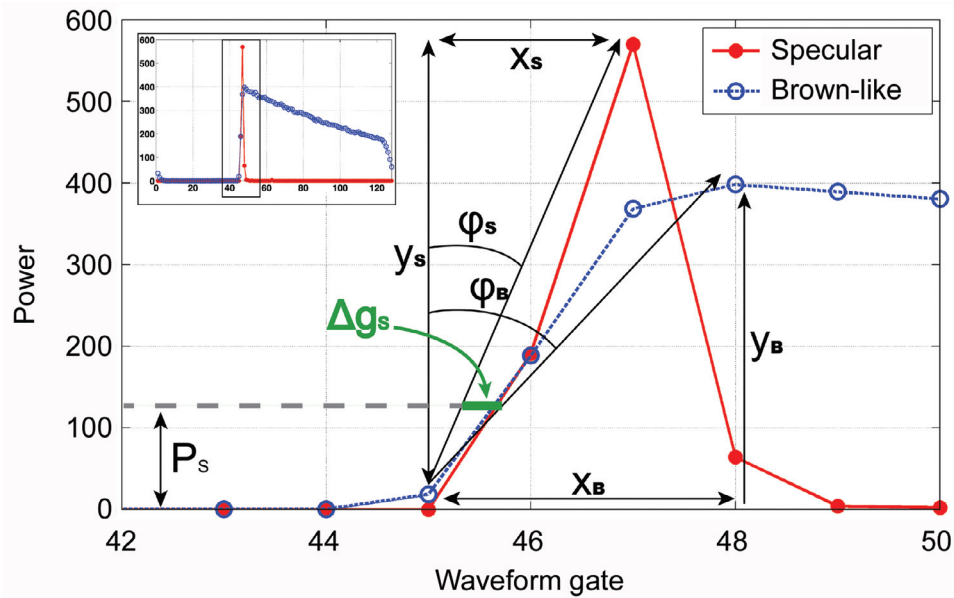

Fig. 5. A conceptual illustration of a retracking gate correction (Δg_S) demonstrated by a referenced Brown-like shape measured over water and a specular shape waveform measured over a frozen lake surface. An example (not to-scale) of power threshold (P_S, gray dashed line) meets two slopes at a different gate in abscissa as a retracked gate difference Δg_S (green) is observed during waveform retracking process.

in the physical model during waveform retracking process is needed to address the problem for the seasonally ice-covered Qinghai Lake.

In Brown's average impulse response, altimetry waveform $W(t)$ received in time is a convolution process of three components shown in Eq. (1): instrument point target response (*PTR*), surface elevation probability density function (*PDF*) of the specular points, and average flat surface (or smooth sphere) impulse response (*FS*).

$$W(t) = FS(t) \otimes PTR(t) \otimes PDF(t) \qquad (1)$$

However, the $FS(t)$ term given in Eq. (2) from Brown (1977) with σ_o term treated as a constant in the original form ignores the extreme scattering characteristics in $FS(t)$ due to its ocean-oriented assumption for the surface whose mean-square slope (MSS) is a Gaussian distribution and has a limited range. In Dinardo and Benveniste (2009), it is assumed that the scattering process in inland water and coastal

zones potentially varies the trailing edge slope of the *FS* model, by adjusting parameters in the scattering term, and eventually affects the convoluted waveforms.

$$FS(t) = \frac{\lambda^2}{(4\pi)^3 L_p} \int_{At} \frac{\delta\left(t - \frac{2R}{c}\right) G^2(\theta, \omega) \sigma_o(\psi, \phi)}{R^4} dA \quad (2)$$

where

λ = radar carrier wavelength;
L_P = two-way signal propagation loss;
c = the speed of light in vacuum;
t = impulse two-way travel time;
R = range from the illuminated element to the radar;
$G(\theta, \omega)$ = gain of the radar antenna as a function of relative angle to the boresight;
$\sigma_o(\psi, \phi)$ = surface backscatter cross section as a function of relative angle to the radar subnadir;
dA = elemental scattering area;
At = total illuminated area.

The radar backscatter cross section (RBCS) σ_o at the incidence angle is obtained from Liu et al. (2000):

$$\sigma_o(0) = \frac{|R(0)|^2}{2\sigma_u \sigma_c} = \frac{|R(0)|^2}{2s^2} \quad (3)$$

where

$|R(0)|^2$ = Fresnel reflection coefficient for normal incidence;
σ_u, σ_c = upwind and crosswind components of RMS slope;
s^2 = mean-square slope.

For a smooth surface with a least surface standard deviation, the energy of σ_o tends to become more concentrated without loss in scattering. Here, we suspect that the lake ice, or even calm water surface with least roughness, could generate anomalous waveform returns. Therefore, this unmodeled scattering characteristic should be considered in quasi-specular cases and a correction to the track offset is required to avoid overestimations in the surface height retrieval, which is due to a shift of the waveform peak to the center of nominal tracking gate.

In the following sections, we first collected Envisat retracked height and waveform data over Qinghai Lake. We then inspected lake surface condition by analyzing remote sensing imagery at the time close to the altimetry measurements to ensure the absence of snow accumulation and scrutinize the possible timing of ice returns. After filtering out the quasi-specular shape of waveform from a series of waveform classification algorithm, we then developed an empirical gate transition based on the relative leading edge slopes between specular and Brown-like waveforms, towards com-

puting a gate correction for the threshold retracker (TR). In the following section, various retracked heights compared to *in situ* gauge data are summarized in terms of root-mean-square error (RMSE) and correlation coefficients. It should be noted that only 20% level of TR followed by a 20% peak energy for gate correction computation is presented in the result since the fewer (10%) and higher (50%) threshold settings were tested to yield an under- and over-estimation of corrections to the measurements, respectively. The optimum threshold level for the computing gate correction needs further study on scattering properties, e.g., surface- or volume-scattered characteristic (Davis 1997), for lake ice.

2. DATA AND METHOD

2.1 Envisat Altimetry and Lake Gauge Data

Envisat was launched by the European Space Agency (ESA) in August 2002, following two successful predecessors ERS-1/-2 missions in the 1990s. The altimetry instrument onboard Envisat is to synoptically monitor large-scale ocean surface topography, ice sheet elevation change, sea ice freeboard height change, hydrology and land cover studies. Envisat carries a suite of instruments including a dual-frequency (Ku and S-band) radar altimeter (RA2) and other instruments such as an advanced synthetic aperture radar and radiometers. Operating in a sun-synchronous orbit with a 35-day repeat cycle, the radar altimeter onboard Envisat not only facilitates geophysical and oceanic studies by observing ocean circulation and sea-level in the open ocean, but also covers many inland water bodies under its dense cross-track interval (~80 km at the Equator). Each bin (or gate) of the Envisat Ku-band (13.6 GHz) waveform (128 bins) has a time resolution of 3.125 nanoseconds based on the maximum resolution setting of the 320 MHz bandwidth. In this study, we used both the Envisat RA2 Geophysical Data Record (RA2_GDR_2P) and Sensor Data Record (RA2_MWS_2P) over 2003 - 2009 (cycles 12 - 84) within a data span when the *in situ* Qinghai Lake gauge data were available. Here the Qinghai Lake gauge data are digitized from Zhang et al. (2011a, b) and Wang et al. (2012, 2013). An ascending pass #240 between 36.9 - 37.1°N and a descending pass #276 between 36.73 - 36.79°N were obtained. The latitudinal box (> 6 km from coasts) for each pass was selected to prevent possible land contamination in the coastal waveforms (Deng et al. 2002). Moreover, other onboard retrackers including ICE-1, ICE-2, SEAICE and OCEAN were used to evaluate conventional retracked results without gate correction inferring the existence of specular waveforms. Each retracked height had later been applied with necessary instrumental and environmental corrections since the media between the space-borne radar altimeter and the surface are non-homogeneous that substantively advance or delay the transmitted signals (Lee et al. 2010). These corrections are known as Doppler shift and oscillator drift for in-

strumental corrections, ionosphere and dry/wet troposphere for media corrections, and solid Earth tide and pole tide for geophysical corrections.

2.2 Remote Sensing Imagery and the Normalized Difference Snow Index (NDSI)

To verify the *in situ* condition of lake surface and check the possible snow accumulation during winter to early spring, we acquired two of NASA's imaging series: (1) Earth Observing-1 Mission (EO-1) with Advanced Land Imager (ALI) spectrometer (Sherwood et al. 2006), and (2) the Landsat series TM/ETM+ (Enhanced Thematic Mapper Plus) multispectral scanning. Both instruments have been used to measure land cover and its changes by means of characterizing different optical properties between specific features in the image. These two sensors' reflectance data are publicly available from the USGS *EarthExplorer* website (http://earthexplorer.usgs.gov).

The EO-1 ALI, launched in November 2000 was operational in a circular orbit at an altitude of ~705 km with simultaneous measurement of nine different wavelengths. Each band of ALI has 30 m spatial resolution for multispectral and 10 m for panchromatic imagery (Burke et al. 2004). On the other hand, Landsat 7 data with functioning Scan Line Corrector (SLC) before May 2003 as well as Landsat 4-5 TM image over 2003 - 2009 were examined over Qinghai Lake. The Digital Numbers (DNs) of both imagery sets have been converted to spectral reflectance via calibration coefficients (Chander et al. 2009). The Normalized Differ-

ence Snow Index (NDSI) of both data sets was then computed to roughly discriminate ice-water-land ratio by using two bands near 0.56 and 1.65 µm given as follows (Valovcin 1976):

$$NDSI = \frac{\rho_{0.56} - \rho_{1.65}}{\rho_{0.56} + \rho_{1.65}} \tag{4}$$

where

$\rho_{0.56}$ = band 2;
$\rho_{1.65}$ = band 5 for both sensors.

An example of NDSI showing snow/ice extent and its disturbance to the altimetry backscattering coefficient (BC) is displayed in Fig. 6. The EO-1 ALI image on 21 March 2004 shows a part of lake was still frozen during the early spring and caused fluctuation in BCs while the along-track altimetry footprints encountered dispersed ice floes. The bloom in BCs confirms that the specular echoes as shown in Fig. 5 originated from non-water surface. Based on an experimental NDSI threshold (Griffin et al. 2005; Doggett et al. 2006) for classification (approximate water < 0.4), we note that the delineation of lake ice boundary matches fairly well as shown by a false-color image (Fig. 6b). The accumulation of fresh snow is further interpreted from the highest value in NDSI and inferred from surrounding land cover. After a deliberative inspection and computation of the NDSI for available winter images, we conclude that the lake surface is seldom covered by snow presumably due to a semiarid climate (Chu et al. 2007) in this region of the Tibetan Plateau which has an average of < 5 cm snow depth
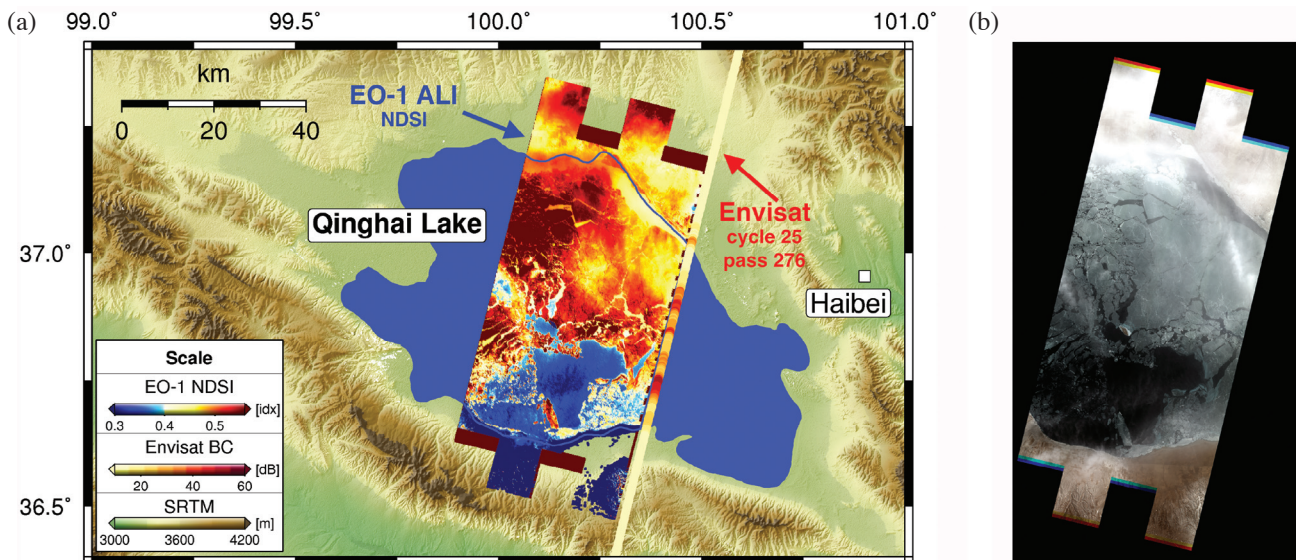

Fig. 6. (a) Lake ice/snow extent estimated by NDSI is computed from EO-1 ALI imagery on 03/21/2004. Envisat pass #276 color-coded by a backscattering coefficient (BC) was measured on 03/28/2004. The higher values of BC than normal water surface return (15 - 20 dB) fluctuate while satellite ground track overpasses ice floes. Background relief is scaled by C-band SRTM3 DEM. (b) False-color images composed by ENVI software are computed from original multispectral imagery (R: Band 3, G: Band 2, B: Band 1), with approximate cloud coverage 30 - 39% mostly in the upper part.

in winter and < 30 days of snow-cover per year (Che et al. 2008). Therefore, it is appropriate to assume that the inaccurate measurements during winter are influenced by icy surface rather than snow layers. The latter case could have resulted in higher Envisat lake level measurements during winter time.

2.3 Processing Method: Waveform Classification and Retracking Gate Correction

As mentioned before, Fig. 5 demonstrates a typical specular waveform that has sharper leading edge and a sudden drop of trailing edge than the Brown-like shape. Therefore, it is postulated a correction applied to the tracking offset by means of a differentiated slope in between in order to improve the height estimate. The first step of this process is to set up a series of criteria to identify waveforms encountering ice contamination. These criteria were derived from a reference of echoes presumably returned from water surface, i.e., picking one summer cycle per year over 2003 - 2010 and then averaging the waveform amplitude. As demonstrated by four along-track average waveforms selected in different months, Fig. 7 depicts the echo from water surface is similar in leading/trailing edge formation. Therefore, the difference of waveform parameters between water seasons is disregarded and the averaged waveform is treated as the prototypical return from local water surface. Several constraints were thus made in advance to identify quasi-specular feature among all surface echoes in an automatic fashion: (1) BC value exceeds 15 dB, (2) waveform COG, in terms of gate, located prior to 75, and (3) peak amplitude must exceed 400 power units. Only waveforms matching these criteria were then applied the gate correction after a standard 20% threshold retracking process (Davis 1997). The next step is to estimate the correction in number of gates needed for the picked waveform samples. This transition is related to the difference in the inverse of the slope of the leading edge compared to the reference. Here we define the inverse of slope is the unit length of peak width (in gate) divided by the unit length of peak amplitude (in power unit) which is equal to the tangent of azimuth angle of each leading edge. The gate correction term, Δg_S, as denoted in the geometry of Fig. 5 is then described as:

$$\Delta g_S = P_S \times (\tan \varphi_B - \tan \varphi_S) = P_S \times \left(\frac{x_B}{y_B} - \frac{x_S}{y_S} \right) \qquad (5)$$

where subscripts S and B denote Specular waveform and Brown-like reference, respectively, and

Δg_S = number of gate to be corrected for specular waveforms;

P_S = power level computed from 20% energy of peak in the specific specular waveform;

φ = zenith angle of leading edge;

x = unit length of gate difference between rising gate and the peak;

y = unit length of power difference between rising gate and the peak amplitude.

Given by the reference waveform, a typical leading edge at this region has a peak amplitude of ~400 power units and a width across 4 gates. Thus the inverse slope of leading edge x_B/y_B is treated as a constant approximately 0.01. This assumption is legitimate in this case study as the wind speed at Qinghai Lake is relatively low and consistent over a multi-year evaluation (Qin and Huang 1998) which presumably yields less inter-annual or seasonal signals in the significant wave height (SWH) that affects the slope of waveform leading edge. On the other hand, since we only propose a correctional term for the threshold retracker that focuses on the leading edge part of a waveform, other parameters such as backscatter coefficient and the trailing edge slope is negligible in this technical process. Finally, the corrected 20% TR retracked height is expressed as:

$$R_S = R - \Delta g_S \times gm \qquad (6)$$

where

R_S = retracked height after applying gate correction [m];

R = original 20% TR retracked height (with instrumental, media, and geophysical corrections);

gm = 0.4684375 (gate to meter conversion parameter, based on 320 MHz bandwidth setting).

In addition, one more constrained setting of gate correction < 1 [gate] is required to accommodate waveforms whose amplitude of occasional boost reaches over a few thousands of power units. The empirical method built in this study depending on the peak amplitude sometimes encounters exaggerated estimate of gate corrections.

3. RESULTS AND DISCUSSIONS

A temporal validation of retracked height using ICE-1, 20% TR (uncorrected) and a corrected 20% TR is shown in Fig. 8 by comparing their water level difference (or level anomaly where the mean in each time series has been removed) with *in situ* gauge data. We observe that both Envisat altimetry passes #240 (Fig. 8a) and #276 (Fig. 8b) using ICE-1 and 20% TR without correction have problematic measurements every winter which yield a double-peak pattern in annual variation and have apparent discrepancies compared to gauge level data (same as Fig. 4). In contrast, the 20% TR applied gate corrections shorten the deviation in between and coincide better with gauge data in seasonal phases. Although few of the corrections are ap-

parently overestimated (e.g., around January 2007 for #240 and similar position for #276), and some of them are less accurately corrected (e.g., around January 2005 and January 2009 for #276), the overall refinement in a least-square sense concludes that the gate corrections essentially amend a major part of inaccurate measurements in winter and preserve reliable accuracy in mid-year. Both passes have a better agreement with gauge data even in summer, due to a lift of time series by subtracting winter bumps that lowers the mean lake level.

A statistical comparison, in terms of RMSE and correlation coefficients among various retrackers is shown in Table 1. The uncertain value after the plus-minus sign in

each entry indicates the internal variability computed from the mean standard deviation of along-track height estimate in each cycle which can be expressed as:

$$\text{uncertainty} = \frac{\sum\limits_{j=1}^{n} \sigma_H(j)}{n} \tag{7}$$

with

$$\sigma_H(j) = \sqrt{\frac{\sum\limits_{c=1}^{k}\left[H(c,j) - \sum\limits_{c=1}^{k} H(c,j)\Big/k\right]^2}{k-1}} \tag{8}$$
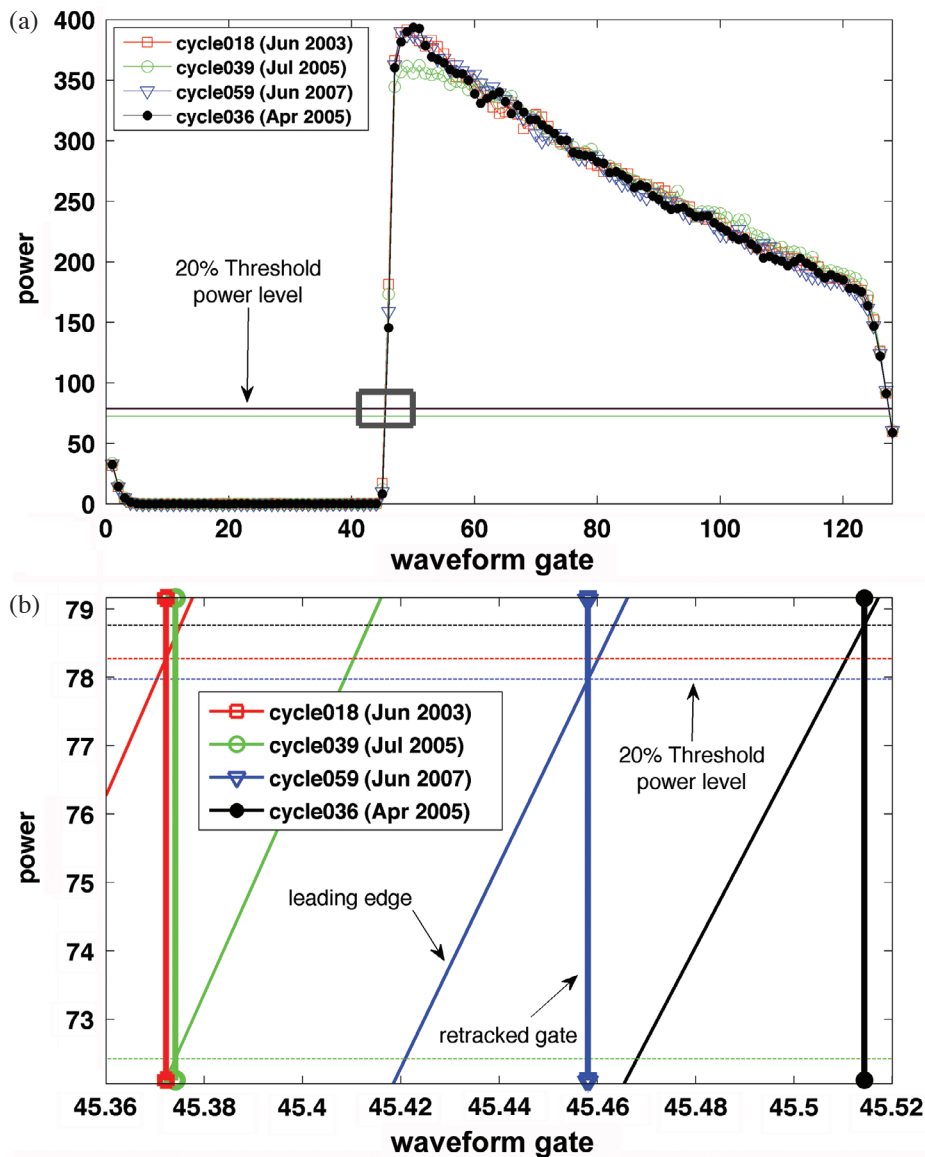

Fig. 7. A demonstration of water waveforms collected over different months. Top: Four waveforms have a similar leading/trailing edge slope and the power level computed from 20% peak power amplitude also located at a comparable level. Bottom: A blow-up view of the retracked gate denoted as a gray box in the top panel. Vertical line indicates the retracked gate obtained from the intersection between 20% threshold power level (horizontal line) and the leading edge. The offset among retracked gates is less than 0.15 (or 7 cm in length equivalent) in given examples.
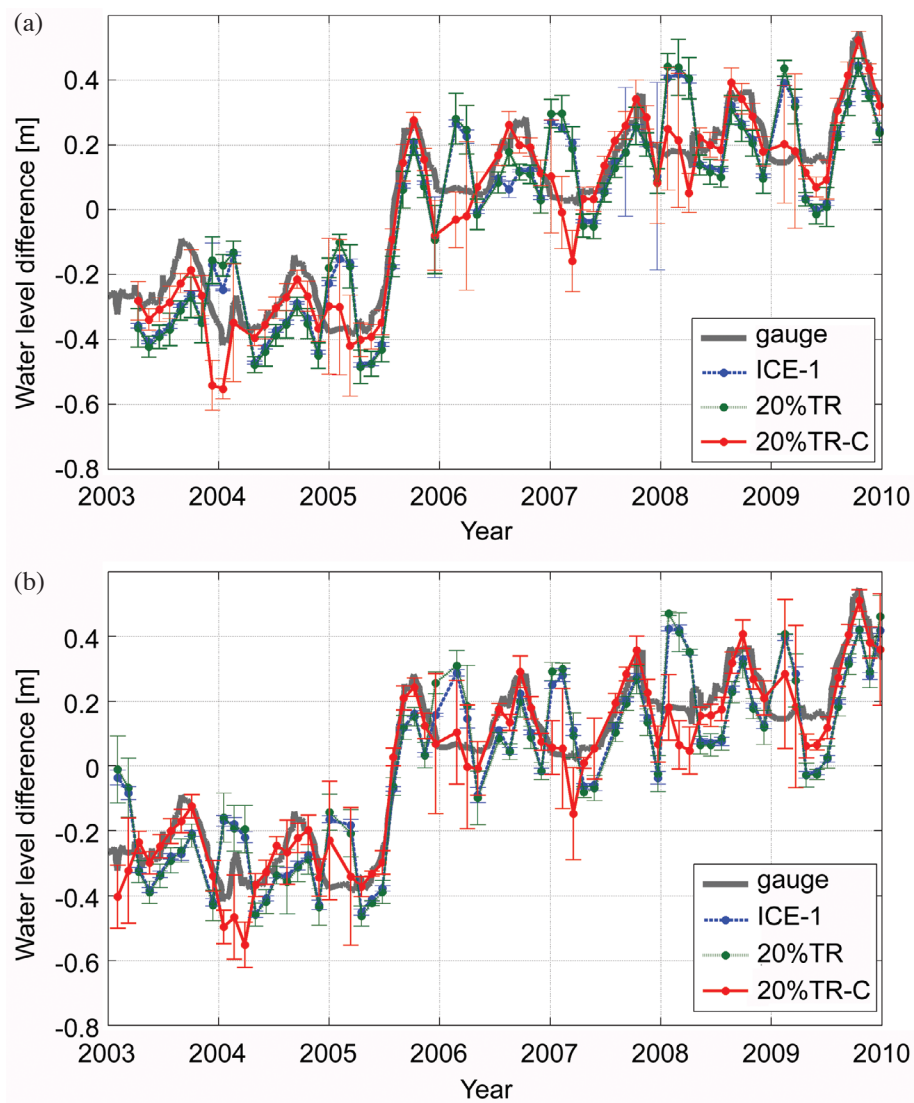
Fig. 8. Top: A comparison of water level variation for Envisat pass #240, between gauge (gray), Envisat ICE-1 (blue), 20% TR without correction (green), and 20% TR after correction (red). Bottom: A similar comparison for Envisat pass # 276.

Table 1. Statistics of RMSE and correlation coefficient compared among different radar altimeter waveform retrackers and lake gauge data.

Retracker	Pass #240 (lat: 36.9 - 37.1°N)		Pass #276 (lat: 36.73 - 36.79°N)	
	RMSE [cm]	Correlation	RMSE [cm]	Correlation
ICE-1	13 ± 2	0.87	14 ± 1	0.86
ICE-2	17 ± 2	0.79	17 ± 2	0.80
SEAICE	19 ± 5	0.76	19 ± 3	0.76
OCEAN	39 ± 4	0.40	37 ± 4	0.45
20% TR (uncorrected)	15 ± 4	0.85	15 ± 4	0.84
20%TR (corrected)	6 ± 7	0.98	6 ± 7	0.97

where

n = number of valid cycles for certain passes #240 and #276;

$H(c, j)$ = retracked height computed from c^{th} waveform in j^{th} cycle;

k = number of waveforms within selected spatial box.

To assess the performance between retrackers in the following discussion we use an improvement percentage (IMP) factor introduced in Hwang et al. (2006):

$$IMP = \frac{\sigma_{compared} - \sigma_{comparing}}{\sigma_{compared}} \times 100(\%) \qquad (9)$$

where σ is the RMSE of each retracker's estimate against gauge data.

For pass #240, the corrected 20% TR with 6 cm RMSE has significant improvement over ICE-1 (13 cm, IMP = 54%), ICE-2 (17 cm, 65%), SEAICE (19 cm, 68%), OCEAN (39 cm, 85%), and is better than uncorrected 20% TR (15 cm, 60%). The improvement is also noted in the enhanced correlation (0.98) compared with gauge time series. Similarly, pass #276 with a shorter range of along-track measurements, between latitude 36.73°N - 36.79°N (about 6.8 km, corresponding to ~18 points for 18-Hz data in each cycle) has almost identical results with #240 among compared retrackers. The corrected 20% TR outperform other retrackers at least 57% in RMSE and > 0.11 improvement in correlation. We conclude that the empirical gate corrections developed in this study efficiently suppressed the effects of spurious signals in winter and at the same time, increase the accuracy in other seasons when sporadic specular waveforms also have chances to occur. However, an increase of uncertainty is also noticed in the corrected time series. This problem may be due to a fluctuation of correction for a series of waveforms that have inconsistent peak amplitudes as we can observe in Fig. 3b. As a subject of future work, a more sophisticated technique to accommodate the instability of peak values could potentially further improves the accuracy in the along-track measurements.

4. CONCLUSIONS

Current retrackers developed for radar altimetry waveforms are primarily designed for Brown-like (OCEAN) or multi-peaks (ICE) echoes by using several fitting parameters. However, there are only limited algorithms dedicated to waveform classification and retrackers for the occurrence of numerous return waveform shapes. Recent developments of radar altimeter retracking algorithms include adaptive retracking (e.g., Wang et al. 2010) or sub-waveform extraction (Yang et al. 2010, 2011, 2012), and the algorithms described in the PISTACH project (Gómez-Enri et al. 2008;

Vignudelli et al. 2009). These algorithms are intended to potentially extend radar altimeter data coverage toward the coastlines, in circumpolar seas, and over inland water bodies. In this study, we demonstrate a viable algorithm to effectively identify quasi-specular waveforms for ice-contaminated data and use adjacent waveform samples to estimate the lake surface height at the seasonally ice-covered Qinghai Lake. The improved retrieval of radar altimeter elevation measurements over an alpine lake like the Qinghai Lake benefits studies in atmosphere and hydrology. Although this technique is hitherto only experimentally verified at the study region, it is envisioned that the method could be effectively applied to other alpine lakes with similar seasonally surface changes, to improve the accuracy of radar altimetry lake level measurements. The only prerequisite condition for the target area is less snow accumulation year-round as the penetration depth of electromagnetic radiation in the snow layers is still difficult to model. Further research applying this technique to other regions is needed to improve the robustness of the algorithm developed in this study.

REFERENCES

Bamber, J. L., 1994: Ice sheet altimeter processing scheme. *Int. J. Remote Sens.*, **15**, 925-938.

Berry, P. A. M., J. D. Garlick, J. A. Freeman, and E. L. Mathers, 2005: Global inland water monitoring from multi-mission altimetry. *Geophys. Res. Lett.*, **32**, L16401, doi: 10.1029/2005GL022814. [Link]

Birkett, C. M., 1995: The contribution of TOPEX/POSEIDON to the global monitoring of climatically sensitive lakes. *J. Geophys. Res.*, **100**, 25179-25204, doi: 10.1029/95JC02125. [Link]

Brown, G., 1977: The average impulse response of a rough surface and its applications. *IEEE Trans. Antennas Propag.*, **25**, 67-74, doi: 10.1109/TAP.1977.1141536. [Link]

Burke, H., S. Hsu, M. Griffin, C. Upham, and K. Farrar, 2004: EO-1 hyperion data analysis applicable to cloud detection, coastal characterization and terrain classification. Geoscience and Remote Sensing Symposium, IGARSS '04 Proceedings, 2004 IEEE International,

vol. 2, 1483-1486, doi: 10.1109/IGARSS.2004.13687 01. [Link]

Calmant, S. and F. Seyler, 2006: Continental surface waters from satellite altimetry. *C. R. Geosci.*, **338**, 1113-1122, doi: 10.1016/j.crte.2006.05.012. [Link]

Chander, G., B. L. Markham, and D. L Helder, 2009: Summary of current radiometric calibration coefficients for Landsat MSS, TM, ETM+, and EO-1 ALI sensors. *Remote Sens. Environ.*, **113**, 893-903, doi: 10.1016/j.rse.2009.01.007. [Link]

Che, T., X. Li, R. Jin, R. Armstrong, and T. Zhang, 2008: Snow depth derived from passive microwave remote-sensing data in China. *Ann. Glaciol.*, **49**, 145-154, doi: 10.3189/172756408787814690. [Link]

Che, T., X. Li, and R. Jin, 2009: Monitoring the frozen duration of Qinghai Lake using satellite passive microwave remote sensing low frequency data. *Chin. Sci. Bull.*, **54**, 2294-2299. doi: 10.1007/S11434-009-0044-3. [Link]

Chu, Y. H., J. Li, W. P. Jiang, X. C. Zou, X. Y. Xu, and C. B. Fan, 2007: Determination of inland lake level and its variations in China from satellite altimetry. In: Tregoning, P. and C. Rizos (Eds.), Dynamic Planet - Monitoring and Understanding a Dynamic Planet with Geodetic and Oceanographic Tools, vol. 130, 80-83, International Association of Geodesy Symposia, Cairns, Australia, 22-26 August 2005.

Davis, C. H., 1997: A robust threshold retracking algorithm for measuring ice-sheet surface elevation change from satellite radar altimeters. *IEEE Trans. Geosci. Remote Sensing*, **35**, 974-979, doi: 10.1109/36.602540. [Link]

Deng, X., W. E. Featherstone, C. Hwang, and P. A. M. Berry, 2002: Estimation of contamination of ERS-2 and POSEIDON satellite radar altimetry close to the coasts of Australia. *Mar. Geodesy*, **25**, 249-271, doi: 10.1080/01490410214990. [Link]

Dinardo, S. and J. Benveniste, 2009: Application of a modified Brown model to Quasi-specular echoes. Third Coastal Altimetry Workshop, Frascati, Italy, 17-18/09/09.

Doggett, T., R. Greeley, S. Chien, R. Castano, B. Cichy, A. G. Davies, G. Rabideau, R. Sherwood, D. Tran, V. Baker, J. Dohm, and F. Ip, 2006: Autonomous detection of cryospheric change with hyperion on-board Earth observing-1. *Remote Sens. Environ.*, **101**, 447-462, doi: 10.1016/j.rse.2005.11.014. [Link]

Frappart, F., S. Calmant, M. Cauhopé, F. Seyler, and A. Cazenave, 2006: Preliminary results of ENVISAT RA-2 derived water levels validation over the Amazon basin. *Remote Sens. Environ.*, **100**, 252-264, doi: 10.1016/j.rse.2005.10.027. [Link]

Fu, L. L. and A. Cazenave, 2001: Satellite Altimetry and Earth Sciences, Volume 69: A Handbook of Techniques and Applications (International Geophysics), Academic Press, 463 pp.

Gómez-Enri, J., P. Cipollini, C. Gommenginger, C. Martin-Puig, S. Vignudelli, P. Woodworth, J. Benveniste and P. Villares, 2008: COASTALT: improving radar altimetry products in the oceanic coastal area. In: Bostater, C. R., S. P. Mertikas, X. Neyt, and M. Velez-Reyes, (Eds.), Remote Sensing of the Ocean, Sea Ice, and Large Water Regions 2008, (Conference Volume 7105), Cardiff, Wales, United Kingdom, September 15, 2008, doi: 10.1117/12.802456. [Link]

Griffin, M. K., S. M. Hsu, H. K. Burke, S. M. Orloff, and C. A. Upham, 2005: Examples of EO-1 Hyperion Data Analysis. *Lincoln Lab. J.*, **15**, 271-298.

Hwang, C., J. Guo, X. Deng, H. Y. Hsu, and Y. Liu, 2006: Coastal gravity anomalies from retracked Geosat/GM altimetry: Improvement, limitation and the role of airborne gravity data. *J. Geodesy*, **80**, 204-216, doi: 10.1007/S00190-006-0052-X. [Link]

Hwang, C., Y. C. Kao, and N. Tangdamrongsub, 2011: A Preliminary analysis of lake level and water storage changes over Lakes Baikal and Balkhash from satellite altimetry and gravimetry. *Terr. Atmos. Ocean. Sci.*, **22**, 97-108, doi: 10.3319/TAO.2010.05.19.01(TibXS). [Link]

Idris, N. and X. Deng, 2011: Waveform retracking techniques for quasi-specular and multi-peaked echoes near the coast. 5th Coastal Altimetry Workshop 16-18 October 2011, San Diego, USA.

Jiang, W., Y. Chu, J. Li, and Y. Yao, 2008: Water level variation of Qinghai Lake from altimeteric data. *Geomatics Infor. Sci. Wuhan Univ.*, **33**, 64-67.

Koster, R. D., P. R. Houser, E. T. Engman, and W. P. Kustas, 1999: Remote sensing may provide unprecedented hydrological data. *Eos, Trans., AGU*, **80**, 156-156, doi: 10.1029/99EO00112. [Link]

Kuo, C. Y. and H. C. Kao, 2011: Retracked Jason-2 altimetry over small water bodies: Case study of Bajhang River, Taiwan. *Mar. Geodesy*, **34**, 382-392, doi: 10.1080/01490419.2011.584830. [Link]

Kwok, R., G. F. Cunningham, M. Wensnahan, I. Rigor, H. J. Zwally, and D. Yi, 2009: Thinning and volume loss of the Arctic Ocean sea ice cover: 2003-2008. *J. Geophys. Res.*, **114**, C07005, doi: 10.1029/2009JC005312. [Link]

Lee, H., C. K. Shum, Y. Yi, A. Braun, and C. Y. Kuo, 2008: Laurentia crustal motion observed using TOPEX/POSEIDON radar altimetry over land. *J. Geodyn.*, **46**, 182-193, doi: 10.1016/j.jog.2008.05.001. [Link]

Lee, H., C. K. Shum, W. Emery, S. Calmant, X. Deng, C. Y. Kuo, C. Roesler, and Y. Yi, 2010: Validation of Jason-2 altimeter data by waveform retracking over California coastal ocean. *Mar. Geodesy*, **33**, 304-316, doi: 10.1080/01490419.2010.488982. [Link]

Lee, H., C. K. Shum, K. H. Tseng, J. Y. Guo, and C. Y. Kuo, 2011: Present-day lake level variation from Envisat

altimetry over the northeastern Qinghai-Tibetan Plateau: Links with precipitation and temperature. *Terr. Atmos. Ocean. Sci.*, **22**, 169-175, doi: 10.3319/TAO.2010.08.09.01(TibXS). [Link]

Lee, H., C. K. Shum, I. M. Howat, A. Monaghan, Y. Ahn, J. Duan, J. Y. Guo, C. Y. Kuo, and L. Wang, 2012: Continuously accelerating ice loss over Amundsen Sea catchment, West Antarctica, revealed by integrating altimetry and GRACE data. *Earth Planet. Sci. Lett.*, **321-322**, 74-80, doi: 10.1016/j.epsl.2011.12.040. [Link]

Liu, Y., M. Y. Su, X. H. Yan, and W. T. Liu, 2000: The mean-square slope of ocean surface waves and its effects on radar backscatter. *J. Atmos. Ocean. Technol.*, **17**, 1092-1105, doi: 10.1175/1520-0426(2000)017<1092:TMSSOO>2.0.CO;2. [Link]

Martin, T. V., H. J. Zwally, A. C. Brenner, and R. A. Bindschadler, 1983: Analysis and retracking of continental ice sheet radar altimeter waveforms. *J. Geophys. Res.*, **88**, 1608-1616, doi: 10.1029/JC088iC03p01608. [Link]

Qin, B. and Q. Huang, 1998: Evaluation of the climatic change impacts on the inland lake - A case study of Lake Qinghai, China. *Clim. Change*, **39**, 695-714, doi: 10.1023/A:1005319616456. [Link]

Sherwood, R., S. Chien, D. Tran, B. Cichy, R. Castano, A. Davies, and G. Rabideau, 2006: Autonomous science agents and sensor webs: EO-1 and beyond. Proceeding of: Aerospace Conference, 2006 IEEE, doi: 10.1109/AERO.2006.1655769. [Link]

Shum, C. K., J. C. Ries, and B. D. Tapley, 1995: The accuracy and applications of satellite altimetry. *Geophys. J. Int.*, **121**, 321-336, doi: 10.1111/j.1365-246X.1995.tb05714.x. [Link]

Shum, C. K., Y. Yi, K. Cheng, C. Kuo, A. Braun, S. Calmant, and D. Chambers, 2003: Calibration of JASON-1 altimeter over Lake Erie special issue: Jason-1 calibration/validation. *Mar. Geodesy*, **26**, 335-354, doi: 10.1080/714044525. [Link]

Valovcin, F. R., 1976: Snow/cloud discrimination. Air Force Geophysics Laboratory, AFGL-TR-76-0174, ADA032385.

Vignudelli, S., P. Cipollini, C. Gommenginger, H. Snaith, H. Coelho, J. Fernandes, J. Gómez-Enri, C. Martin-Puig, P. Woodworth, S. Dinardo, and J. Benveniste, 2009: The COASTALT project: Towards an operational use of satellite altimetry in the coastal zone. Proceedings of OCEANS 2009 MTS/IEEE Biloxi Conference, Biloxi, Mississippi, USA, 26-29 October 2009, CD.

Wang, H., Y. Yueh, S. Zhou, and Y. Yang, 2010: Classification of radar altimeter waveforms based on cluster analysis. *Geomatics Inform. Sci. Wuhan Univ.*, **35**, 833-835

Wang, X., X. Cheng, Z. Li, H. Huang, Z. Niu, X. Li, and P.

Gong, 2012: Lake water footprint identification from time-series ICESat/GLAS data. *IEEE Trans. Geosci. Remote Sensing*, **9**, 333-337, doi: 10.1109/Lgrs.2011.2167495. [Link]

Wang, X., P. Gong, Y. Zhao, Y. Xu, X. Cheng, Z. Niu, Z. Luo, H. Huang, F. Sun, and X. Li, 2013: Water-level changes in China's large lakes determined from ICESat/GLAS data. *Remote Sens. Environ.*, **132**, 131-144, doi: 10.1016/j.rse.2013.01.005. [Link]

Wessel, P. P. and W. H. F. Smith, 2010: The Generic Mapping Tools (GMT), Version 4.5.2, Technical Reference and Cookbook.

Wingham, D. J., C. G. Rapley, H. Griffiths, 1986: New techniques in satellite altimeter tracking systems. Proceeding of IGARSS Symposium, Zurich, ESA SP-254.

Wingham, D. J., A. J. Ridout, R. Scharroo, R. J. Arthern, and C. K. Shum, 1998: Antarctic elevation change from 1992 to 1996. *Science*, **282**, 456-458, doi: 10.1126/science.282.5388.456. [Link]

Yang, L., M. Lin, Q. Liu, and D. Pan, 2010: Retracking strategy based on waveform classification and sub-waveform extraction for coastal altimetry along China coastal seas. Geoscience and Remote Sensing Symposium (IGARSS), 2010 IEEE International, 632-635.

Yang, L., M. Lin, Y. Zhang, L. Bao, and D. Pan, 2011: Evaluation of retracking algorithms over China and adjacent coastal seas. In: Vignudelli, S., A. G. Kostianoy, P. Cipollini, and J. Benveniste, (Eds.), Coastal Altimetry, Springer-Verlag Berlin Heidelberg, 2011.

Yang, Y., C. Hwang, H. J. Hsu, E. Dongchen, and H. Wang, 2012: A subwaveform threshold retracker for ERS-1 altimetry: A case study in the Antarctic Ocean. *Comput. Geosci.*, **41**, 88-98, doi: 10.1016/j.cageo.2011.08.017. [Link]

Zhang, G., H. Xie, S. Duan, M. Tian, and D. Yi, 2011a: Water level variation of Lake Qinghai from satellite and *in situ* measurements under climate change. *J. Appl. Remote Sens.*, **5**, 053532, doi: 10.1117/1.3601363. [Link]

Zhang, G., H. Xie, S. Kang, D. Yi, and S. F. Ackley, 2011b: Monitoring lake level changes on the Tibetan Plateau using icesat altimetry data (2003-2009). *Remote Sens. Environ.*, **115**, 1733-1742, doi: 10.1016/j.rse.2011.03.005. [Link]

Zhang, M., H. Lee, C. K. Shum, D. Alsdorf, F. Schwartz, K. H. Tseng, Y. Yi, C. Y. Kuo, H. Z. Tseng, A. Braun, S. Calmant, N. Filizola, and F. Seyler, 2010: Application of retracked satellite altimetry for inland hydrologic studies. *Int. J. Remote Sens.*, **31**, 3913-3929, doi: 10.1080/01431161.2010.483495. [Link]

Zwally, H. J., R. A. Bindschadler, A. C. Brenner, J. A. Major, and J. G. Marsh, 1989: Growth of Greenland ice sheet - Measurement. *Science*, **246**, 1587-1589, doi: 10.1126/science.246.4937.1587. [Link]